Boundary-Layer Meteorol (2008) 129:211–223
DOI 10.1007/s10546-008-9315-9

ORIGINAL PAPER

Wave-Modified Flux and Plume Dispersion in the Stable Boundary Layer

C. J. Nappo · D. R. Miller · A. L. Hiscox

Received: 3 December 2007 / Accepted: 28 August 2008 / Published online: 24 September 2008

Abstract The effects of a pressure jump and a following internal gravity wave on turbulence and plume diffusion in the stable planetary boundary layer are examined. The pressure jump was accompanied by a sudden increase in turbulence and plume dispersion. The effects of wave perturbations on turbulence statistics are analysed by calculating fluxes and variances with and without the wave signal for averaging times ranging from 1 to 30 min. The wave signals are obtained using a band-pass filter. It is shown that second-order turbulence quantities calculated without first subtracting the wave perturbations from the time are greater than those calculated when the wave signal is separated from the turbulence. Estimates of the vertical dispersion of an elevated tracer plume in the stable boundary layer are made using an elastic backscatter lidar. Plume dispersion observed 25 m downwind of the source increases rapidly with the arrival of the flow disturbances. Measured plume dispersion and plume centreline height correlate with the standard deviation of the vertical velocity but not with the wave signal.

Keywords Gravity waves · Planetary boundary layer · Plume dispersion · Reynolds averaging · Turbulence

1 Introduction

Studies by, for example, Einaudi et al. (1989), Nappo (1991), Hauf et al. (1996), Lee and Barr (1998), Rees et al. (2000), Fritts et al. (2003) and Sun et al. (2004) have shown that waves and other disturbances in the nighttime planetary boundary layer (PBL) are common, and that

C. J. Nappo (✉)
CJN Research Meteorology, Knoxville, TN, 37919, USA
e-mail: cjn_met@comcast.net

D. R. Miller
University of Connecticut, Storrs, CT, USA

A. L. Hiscox
Louisiana State University, Baton Rouge, LA, USA

these waves can modify or be a source of turbulence. Conventional turbulence theory is yet to address these effects in an analytical way. Zilitinkevich (2002) has shown that gravity waves could affect long-lived stable boundary layers, and Steeneveld et al. (2008) have demonstrated that wave drag generated by small-scale terrain features could account for turbulence when the Richardson number is greater than a critical value. Intermittent disturbances and waves in the nighttime PBL are often short lived, and persist with varying intensity for tens of minutes (see, for example, Nappo 1991; Sun et al. 2002; Newsom and Banta 2003). In the stable PBL, gravity wave frequencies and the frequencies of the energy-containing turbulence eddies are similar (Finnigan 1988). Thus, wave disturbance energy can be confused with turbulence energy resulting in the over-prediction of second-order turbulence quantities.

The application of statistical plume diffusion models in the stable PBL is problematic when the turbulence is unsteady (Hanna et al. 1982; De Baas and Driedonks 1985; Rao and Nappo 1998). Important parameters in these models are the standard deviations of the vertical velocity, σ_w, and the cross-wind horizontal velocity, σ_v. In operational or field research applications, σ_w and σ_v are often measured in situ. If wave-like perturbations are present, these will contribute to the velocity variances (De Baas and Driedonks 1985), but not to the dispersion. Thus, the measured values of σ_w and σ_v will be inflated, and using them can result in an over-prediction of plume dispersion and an under-prediction of plume concentrations.

The purpose of this paper is to assess the effects of a large-amplitude wave-like disturbance on the vertical fluxes of heat, energy, and momentum, turbulence kinetic energy, horizontal cross-wind velocity variance, and plume dispersion. The wave was observed between 0500 and 0600 mountain daylight time (MDT = UTC + 6 h: all times are MDT) on 21 April 2005 during the Joint Observational Research on Nocturnal Atmospheric Dispersion of Aerosols (JORNADA) study conducted near Las Cruces, New Mexico, U.S.A.

2 Wave-Modified Turbulence

In a series of papers (see e.g., Finnigan and Einaudi (1993) and references therein), the dynamics of wave-turbulence interaction in the stable PBL were studied using a triple-decomposition of the time-dependent variables. As in those studies, we decompose some variable, $q(t)$, into mean $\bar{q}$, turbulence $q'(t)$, and wave $\tilde{q}(t)$ components, i.e.,

$$q(t) = \bar{q} + q'(t) + \tilde{q}(t). \tag{1}$$

In their studies, Finnigan and Einaudi (1993) used the phase-averaging operation introduced by Hussain and Reynolds (1972), i.e.,

$$\langle q(t_i) \rangle = \frac{1}{M} \sum_{j=1}^{M} q(t_i + j\tau), \tag{2}$$

where $\langle\,\rangle$ represents the phase average, t_i is the i'th point in a discrete time series of M points, and τ is the period of the wave. The wave period is best determined by the surface pressure since this is least affected by activity in the PBL and allows a clear determination of wave period (Finnigan 1988). Using the time-averaged value,

$$\bar{q} = \frac{1}{M} \sum_{i=1}^{M} q(t_i), \tag{3}$$

the wavelike part of the signal is given by:

$$\tilde{q}(t_i) = \langle q(t_i) \rangle - \bar{q}, \tag{4}$$

and the turbulence is given by:

$$q'(t_i) = q(t_i) - \bar{q} - \tilde{q}(t_i). \tag{5}$$

Phase averaging requires a linear monochromatic wave with constant and amplitude over many cycles. Such occurrences are rare in the stable PBL, and instead one generally observes a wave with non-constant amplitude lasting only several cycles. To account for changing wave amplitudes, Finnigan (1988) modulated the phase-averaged waveform $\tilde{q}(t_i)$ using a time dependent amplitude function. This amplitude function was constructed from the low frequencies of the Fourier transform of the original series.

In our analysis, we follow Hauf et al. (1996) by isolating $\tilde{q}$ with a band-pass filter of $q(t)$, and use surface pressure data to identify wave activity. A wavelet analysis is performed to estimate the central frequency of the wave. Here we use the Morlet wavelet, which tends to be more discriminating in frequency space than in time space (Torrence and Compo 1998). As a result of this artifact, the timing of events in the wavelet analysis may be uncertain to within a few minutes, but the frequencies of the events will be sharply focused.

Perhaps the greatest difference between filtering and phase averaging is that phase averaging preserves the contributions of the higher harmonics of the wave. However, Finnigan (1988) showed that the first harmonics of $\tilde{u}$ and $\tilde{v}$ (the horizontal velocity components of the wave) generally have less than half the amplitudes of the fundamental modes. Thus, while filtering may overlook these higher-mode contributions, we feel that the simplicity of the method is sufficient for a first-order analysis.

In this study, we examine the energy flux $\overline{p'w'}$, the heat flux, $\overline{\theta'w'}$, the momentum fluxes $\overline{u'w'}$ and $\overline{v'w'}$, the standard deviations of the vertical and cross-wind velocities σ_w and σ_v respectively, and the turbulence kinetic energy (TKE) with and without the wave signal. Removing the wave component of the variables leads to the Reynolds decomposition, i.e.,only turbulence quantities. For example, for some variable $q(t)$, the Reynolds flux is:

$$\overline{q'w'} = \overline{(q - \bar{q} - \tilde{q})(w - \bar{w} - \tilde{w})}. \tag{6}$$

However, if the wave component is not removed, then the turbulence fluxes will contain wave contributions, and we call these values the wave-modified Reynolds fluxes, i.e.,

$$\overline{q'w'} = \overline{(q - \bar{q})(w - \bar{w})}. \tag{7}$$

3 Methods

The JORNADA field campaign was designed to study the dispersion of elevated tracer plumes in the stable PBL and the effects of turbulence intermittency on plume dispersion. Direct measurements of cross-wind plume relative concentration were made using the University of Connecticut elastic backscatter lidar. The measurement technique was used previously in a study of aerial spray movement and dispersion (Hiscox et al. 2006a) and in a study of nighttime plume dispersion above a forest canopy (Hiscox et al. 2006b). The JORNADA field study was conducted in April 2005 at the New Mexico State University spray study site on the United States Department of Agriculture Jornada Desert Research Ranch (32.31 °N, 106.75 °W). The location of the site is illustrated in Fig. 1. The region is relatively flat with

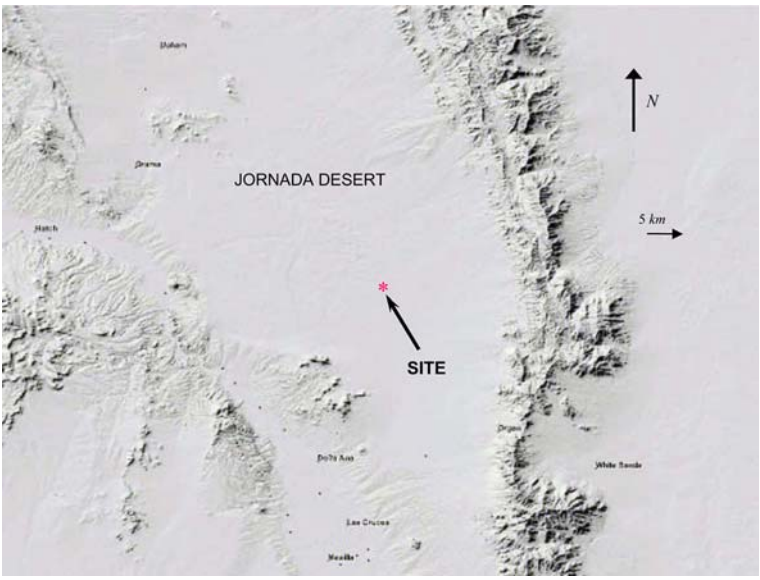

Fig. 1 The JORNADA site

1–2 m tall sparse desert vegetation with an un obstructed fetch in all directions for at least 10 km. The aerodynamic roughness length was estimated to be about 0.06 m.

Figure 2 illustrates the locations of the observation sites. Meteorological instruments were installed and operated by the University of Connecticut (UCONN), National Oceanic and Atmospheric Administration (NOAA), U.S. Army Atmospheric Research Laboratory (ARL), and the Arizona State University (ASU). The UCONN Campbell Scientific CSAT3 sonic anemometers were mounted at 1.5 and 11 m (all heights are above ground level) on a portable mast. In addition, the lower sonic was equipped with a fine-wire thermocouple. A 1-m horizontal square array of four fine-wire thermocouples was mounted at 11 m on the mast, and a Campbell scientific CS500 humidity sensor was located next to the lower sonic anemometer. Three NOAA electronic microbarographs (Setra 520) were installed in an approximately isosceles triangular array near the mast. The base of the triangle, oriented in the east-west direction, was about 100 m long, and the vertex of the triangle was about 65 m south of the mast. A Vaisala DigiCORA tethersonde system and two RM Young 81000 3-axis sonic anemometers were operated by ASU personnel. Profiles of temperature, relative humidity, pressure, wind speed and wind direction were measured up to 250 m. The ASU sonic anemometers were mounted at 1.9 and 2.5 m. The ARL personnel operated its Scintec model FAS Wind Profiler Sodar that measured continuous 10-min average wind speed and wind direction profiles up to about 150 m. The ASU and ARL instruments were located about 500 m west of the UCONN mast. The UCONN sonic and pressure data were recorded at 20 Hz, and the ASU sonic data were recorded at 10 Hz. Doppler sodar winds are reported at 5 m increments above 15 m.

Tracer aerosol plumes were generated using a commercially available fog machine manufactured by Rosco Laboratories, Inc. The machine uses a fluid made of triethylene glycol, propylene glycol, 1,3 butylene glycol and de-ionized water, which is not hazardous to either humans or the environment. The tracer plume release was at 11 m on the UCONN mast. A chimney was used to cool the plume before release to $\pm 1^{\circ}$C of the ambient temperature;

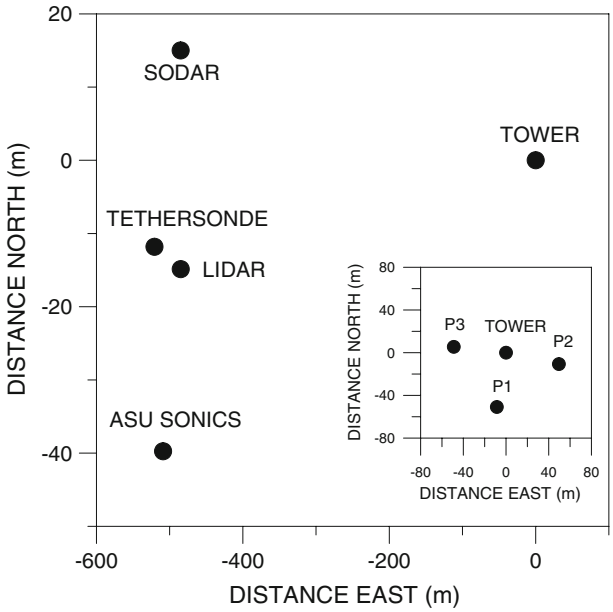

Fig. 2 Instrument layout. Inset shows layout of pressure sensors relative to the tower

however, some initial plume rise or fall did occur. The tracer plume was scanned in a vertical plane with the UCONN scanning elastic-backscatter lidar located about 500 m west of the mast. The lidar has a spatial resolution of 2.55 m, and is configurable to scan in both horizontal and vertical planes, allowing for measurements of the entire plume in about 30 s, or repetitive 3-s measurements of the plume at a fixed downwind location.

Details of the tracer release mechanism and the scanning lidar are given in Hiscox et al. (2006b). Operations began each night at about midnight and continued to about 0630 local time, with vertical cross-sections of the tracer plumes scanned about 26–60 m downwind of the release point depending on wind direction. For the results reported herein, the plume was scanned about 25 m south of the tower.

4 Observations

4.1 Background Flow

The PBL flow on the night of 21 April was highly variable with wind speeds and directions changing over time periods as short as 20 min. Between 0100 and 0200, the winds were fairly steady and from the south-west. Between 0200 and 0300 the winds rotated clockwise about 180 °, and between about 0300 and 0500, winds were light and variable especially below 60 m. At about 0500, the wind shifted to the north-west, and wind speeds increased, and between 0500 and 0520, the winds changed from 1.8 m s^{-1} at 270 ° to 5.4 m s^{-1} at 312 °. From 0520 to 0600, the winds remained fairly uniform. From tethersonde potential temperature profiles we estimate the average depth of the stable PBL to be between 30 and 50 m. Tethersonde wind speed profiles indicated a weak jet at about 40 m between about 0044 and 0150 local time; however, after these times wind speeds decreased.

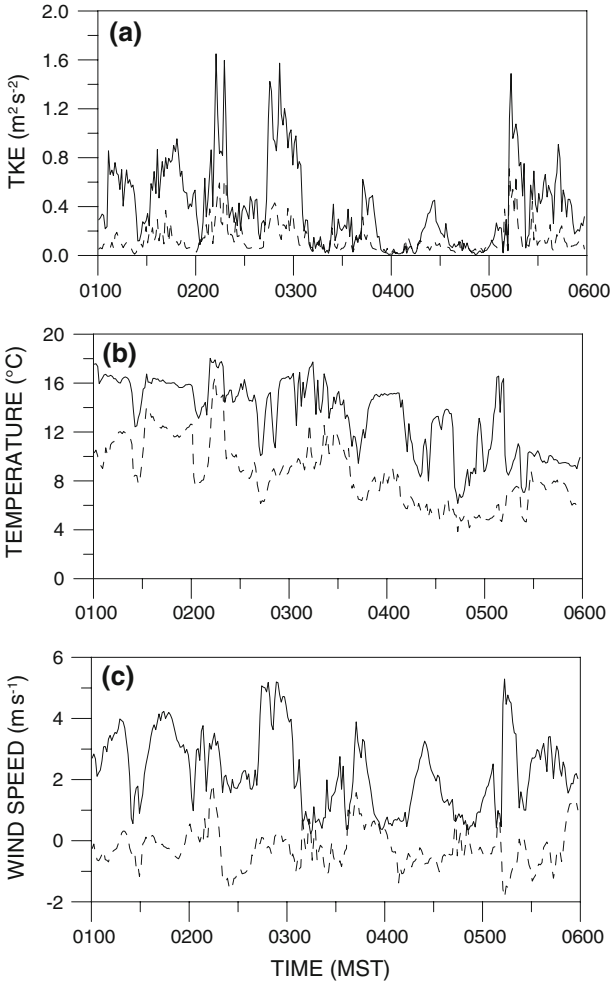

Fig. 3 Time series of TKE (**a**), temperature (**b**), and wind speed (**c**) at 1.5 m (dashed) and 11 m (solid)

Time series of 1-min averaged wind speed, potential temperature, and TKE at 1.5 and 11 m are shown in Fig. 3, where the unsteadiness of the flow is well illustrated. At 11 m, we see a correlation between wind speed and TKE, and also see periods with low temperatures associated with high wind speeds, and periods with high temperatures associated with low wind speeds. At 1.5 m, the average value of z/L between 0100 and 0600 was about 0.11, where L is the Obukhov length scale. Thus, we consider this level to be in the surface layer. After about 0300, the fluctuations in wind speed, potential temperature, and TKE observed at 11 m are either much reduced or absent at 1.5 m. This would indicate that the surface layer was de-coupled from the PBL during these times.

4.2 The Wave Disturbance

Figure 4 shows time variations of 1-s average pressure and temperature at 11 m from 0500 to 0600. Beginning at about 0508:43, the pressure begins to increase, reaching a maximum in about 300 s. At about the same time the temperature decreases from about 16.5 °C to about

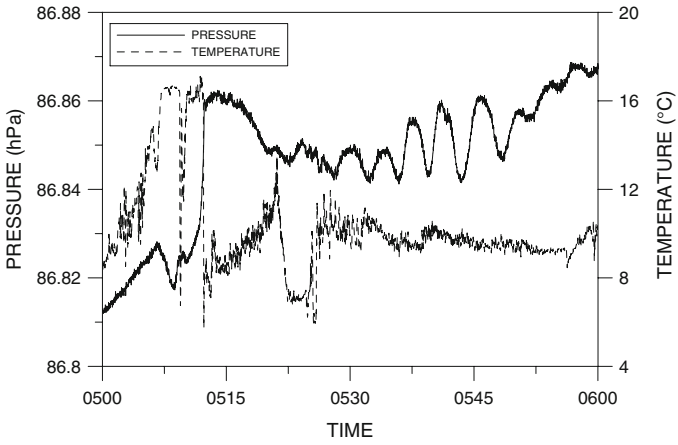

Fig. 4 Surface pressure at south barograph (solid) and temperature at 11 m (dashed)

7.6 °C in a matter of seconds. Using the arrival times of the jumps at the three pressure stations, a lag analysis (Nappo 2002) showed the disturbance to be moving from 313 °with a speed of about 5.4 m s^{-1} and in agreement with the 10-min average sodar winds observed at 15 m between 0510 and 0520. Based on the analysis of Sun et al. (2002) we consider the disturbance to be a density current. At about 0521:07, the first crest of a pressure wave appears at sensor 1, and at about this same time, the temperature reaches a relative maximum of about 12.7 °C. The temperature almost immediately begins to fall reaching a minimum of about 7.1 °C at about 0522:36 which is about the time of the arrival of the pressure wave trough at sensor 1. Between this time and about 0528:21, several high-frequency waves are seen in the temperature and pressure, but after this time, a nearly monochromatic pressure wave develops reaching a maximum amplitude at about 0542. Wave activity continues with decreasing amplitude to about 0600.

Figure 5 shows a wavelet-energy-density analysis of the pressure signal from 0400 to about 0630, the heavy lines defining the cone-of-influence described by Torrence and Compo (1998). Outside of the cone-of-influence, edge effects on the wavelet spectrum become important. The onset of the pressure jump is sharply defined on the 0.5-min disturbance scale, and appears to occur at about 0512. The disturbance energy due to the jump expands through wavelet-scale space, and a region of large wavelet energy density exists with a time scale of about 10 min, similar to the time scale for the pressure jump. Beginning at about 0530, the energy density is confined to a narrow band of disturbance scale (or frequency), a structure that is characteristic of a wave (Hauf et al. 1996). We identify this disturbance with the pressure wave shown in Fig. 4, and estimate the wave period to be about 4 min. Maximum wavelet energy occurs at about 0542 in close agreement with the time series in Fig. 4.

To estimate the characteristics of the wave, the 20-Hz pressure data from the three pressure sensors were averaged into 1-Hz time series. For the 30-min period beginning at 0530, these time series were de-trended, and band-pass filtered to extract the wave component, $\tilde{p_1}$. The band-pass extended over periods from 3 to 5 min. A lag analysis of the pressure time series indicated a wave propagating toward about 090 °at a speed of about 8.7 m s^{-1} , with a horizontal wavelength of about 2090 m and an angular frequency of about 0.026 s^{-1}. If a gravity wave is propagating, then its frequency must be less than the Brunt-Väisälä frequency. The 0438 tethersonde potential temperature profile showed a near-neutral surface layer extending

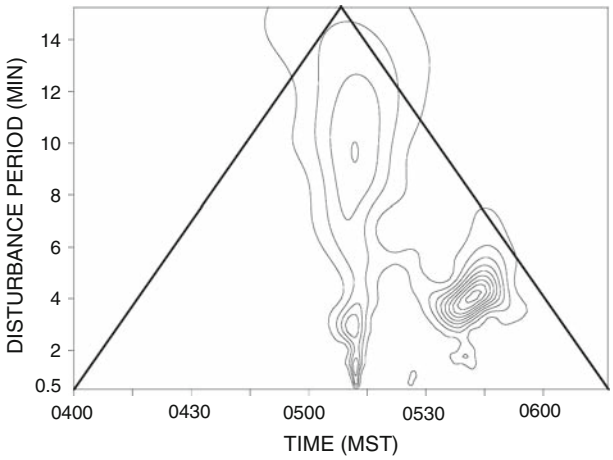

Fig. 5 Wavelet energy density for pressure. Heavy straight lines define the cone-of-influence

up to about 16 m. Above this, the stratification was strongly stable up to about 40 m with the Brunt-Väisälä frequency, N, about 0.10 s^{-1}. From 50 m to about 300 m, $N \approx 0.02\,s^{-1}$. This temperature sounding was made about an hour before the wave event, and assuming the lower PBL continued to cool it seems reasonable to conclude that the wave frequency was less than the Brunt-Väisälä frequency. During the time of the wave event, the 10-min average winds up to about 120 m were toward 120° with speeds not greater than 8 m s^{-1} .

The average amplitude of $\tilde{p}$ was about 0.4 hPa. For comparison, the two waves studied by Finnigan and Einaudi (1993) had pressure amplitudes of about 0.4 and 0.9 hPa; the two mesoscale gravity waves studied by Koch and Golus (1988) had amplitudes of about 4 and 6 hPa. The average amplitude of $\tilde{u}$ was about 0.16 m s^{-1} . For comparison, the waves studied by Finnigan and Einaudi (1993) and Koch and Golus (1988) had velocity amplitudes of about 0.35 and 2.6 m s^{-1} respectively. The wave perturbations $\tilde{p}$ and $\tilde{u}$ were generally in phase, and the correlation coefficient between 0530 and 0600 was about 0.8. These observations support our conjecture that the disturbance is a ducted gravity wave in the PBL.

Wave fluxes were estimated by first averaging the products of the wave variables over consecutive wave periods, and then averaging these over 30 min. The wave energy flux, $\overline{\tilde{p}\tilde{w}}$ was about 2.5×10^{-3} hPa m s^{-1} ; the wave heat flux, $\overline{\tilde{\theta}\tilde{w}}$ was about 0.51 W m^{-2}, and the wave momentum fluxes in the x and y directions were about 2.5×10^{-4} and -31.5×10^{-4} hPa respectively. These values are all about an order of magnitude less than those shown at 20 m in Finnigan and Einaudi (1993). In our case, the average amplitude of $\tilde{w}$ was about 0.02 m s^{-1} while that for Finnigan and Einaudi (1993) was on the order of 0.1 m s^{-1} . This order of magnitude difference may explain the order of magnitude differences in the vertical fluxes.

5 Second-Order Quantities

In this section, we calculate second-order turbulence terms using the Reynolds decomposition (6) and wave-modified Reynolds decomposition (7) at 11 m for averaging times ranging from 1 to 30 min. For each averaging period, linear trends and means were removed from the signals, and the x-axis of the reference coordinate system pointed in the direction of the mean flow.

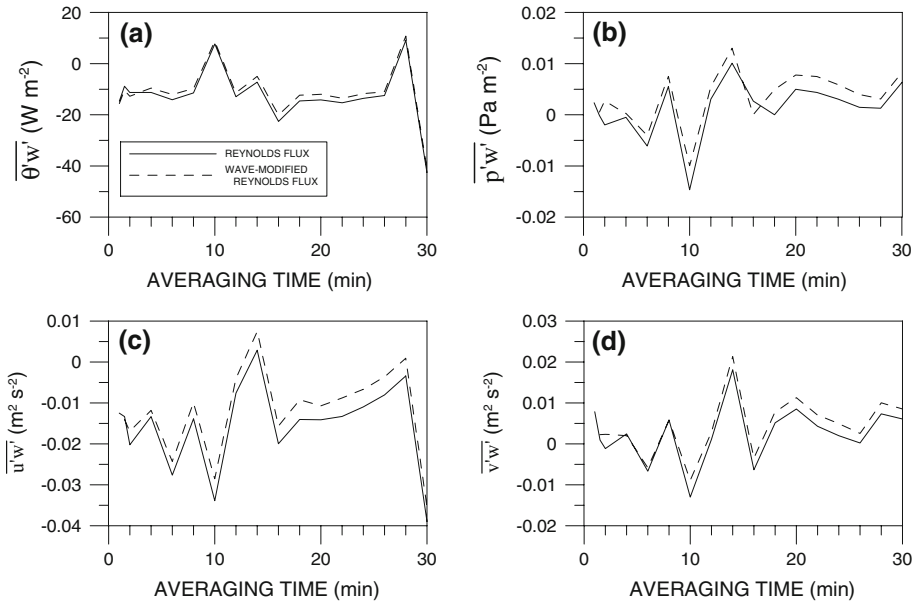

Fig. 6 $\overline{\theta' w'}$ (**a**), $\overline{p' w'}$ (**b**), $\overline{u' w'}$ (**c**), and $\overline{v' w'}$ (**d**) for different averaging times using Reynolds (solid) and wave-modified Reynolds (dashed) decompositions

Figure 6 shows plots of $\overline{\theta' w'}$, $\overline{p' w'}$, $\overline{u' w'}$, and $\overline{v' w'}$ as functions of averaging time. For averaging times greater than 2 min, the wave-modified Reynolds decomposition results in greater (more positive) fluxes and variances. Note that for averaging times less than the wave period (4 min), the wave will contribute little to the wave-modified calculations. Thus, for these times we do not expect to see meaningful differences between (6) and (7). Large variations of the flux values with averaging time generally occur simultaneously using both averaging methods. Accordingly, we surmise that these are due to mesoscale disturbances with time scales greater than the wave period. The peaks and valleys occur at the same averaging times for $\overline{p' w'}$, $\overline{u' w'}$, and $\overline{v' w'}$, and $\overline{\theta' w'}$ appears to be anti-correlated with these variations.

Figure 7 shows plots of TKE, σ_w, and σ_v as functions of averaging time. For TKE and σ_v, the wave-modified Reynolds averaging results in greater values than the turbulence Reynolds averaging; however, there is little difference between these averaging methods when applied to σ_w. Examination of the data shows that the $\tilde{w}$ is about an order of magnitude less than w. Over the 30-min period from 0530 to 0600, the root-mean-square (rms) value of $\tilde{w}$ was about 0.017 m s^{-1} and the rms value of w was about 0.17 m s^{-1} . In contrast, $\tilde{u}$ and $\tilde{v}$ were of the same order as u and v respectively. We note that for σ_w (Fig. 7b) a maximum value occurs at an averaging time of 10 min. The cause of the extreme values of the fluxes at 10-min averaging times is described in Sect. 7.

6 Wave Effects on Plume Dispersion

The effects of the wave disturbance on the tracer plume can be seen in the dispersion parameters derived from the lidar images using the techniques described in Hiscox et al. (2006b). Briefly, we assume that the vertical cross-wind plume concentration distribution is given by:

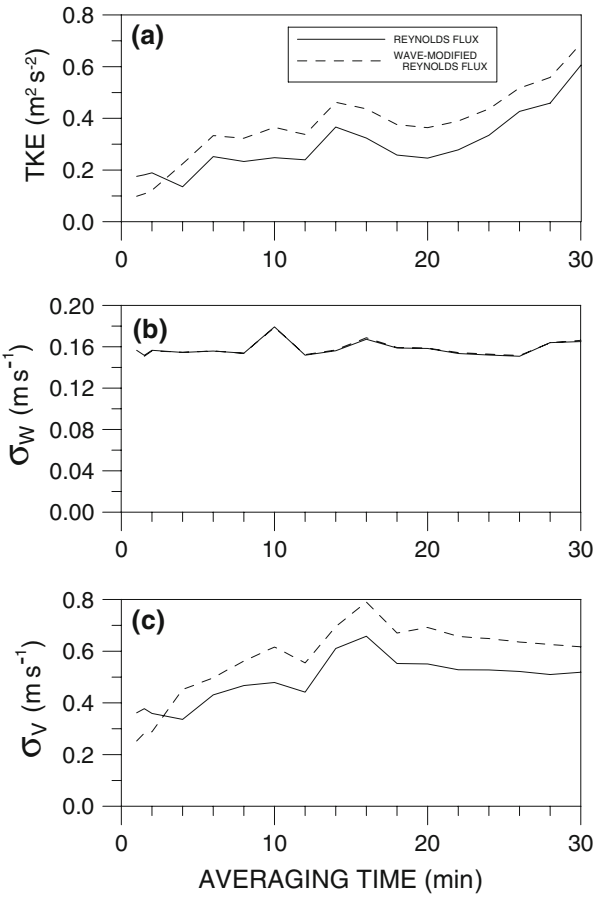

Fig. 7 Same as Fig. 6 but for TKE (**a**), σ_w (**b**), and σ_v (**c**)

$$\chi_E = \chi_M \exp\left(-z_E^2/2\sigma_z^2\right) \tag{8}$$

where χ_E and χ_M are the edge and maximum plume concentration values. Setting $\chi_E = \beta_E$, the lidar backscatter at the 'visible' edge of the plume at distance z_E from the plume centerline, and $\chi_M = \beta_M$, the maximum backscatter value, (8) can be re-written, after Hiscox et al. (2006a), as

$$\sigma_z^2 = \frac{z_E^2}{-2\ln(\beta_E/\beta_M)}. \tag{9}$$

These estimates of σ_z were averaged over consecutive 90-s segments. The time series of σ_z at a downwind distance of about 25 m is shown in Fig. 8 along with 1-s values of w measured at the plume release point. Gaps in the plots of σ_z occur when the lidar was either shut down for data storage purposes or when the plume moved out of the field of view. From a few minutes before 0430 to about 0500, σ_z values are low and relatively steady; the average value is about 0.6 m. At about 0440, wave-like oscillations in w are accompanied by wave-like oscillations in σ_z. The onset of the pressure jump at about 0513 results in a sudden increase in the fluctuations of w (an indication of increased turbulence) accompanied by a sudden rise in σ_z to about 1.5 m. When the wave disturbance appears at about 0520, σ_z jumps in

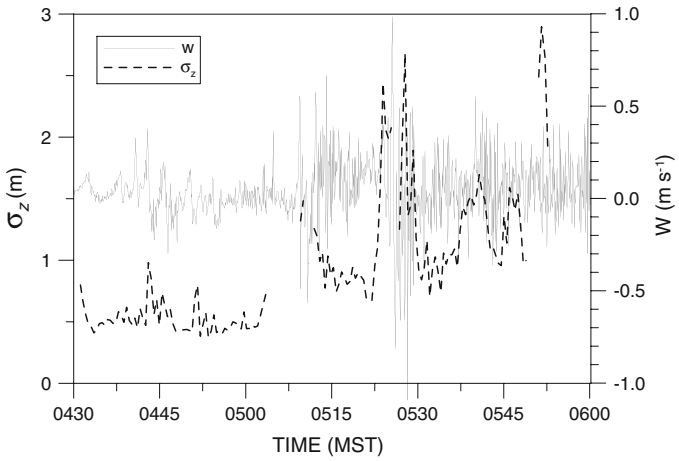

Fig. 8 Time series of w (solid) and σ_z (dashed)

value to about 2.7 m at about 0527 local time. Changes in the values of σ_z appear somewhat associated with changes in the amplitudes of the fluctuations of w, and at about 0552, σ_z reaches its maximum value of about 2.9 m.

For short travel times, T,

$$\sigma_z = \sigma_w T, \tag{10}$$

and our measurements show $\sigma_z \approx 2.7$ m at about 0530. At this time, the wind speed was about 1.5 m s^{-1} . Using observed $\sigma_w \approx 0.17$ m s^{-1} and $T = 17$ s in (10) gives $\sigma_z = 2.9$ m. The good agreement between the measured and calculated σ_z is an indication of the robustness of (10) during nighttime events.

7 Discussion

The origins of the pressure jump or the wave are unknown, and we speculate that the disturbance was a density current, and the wave was generated by wind shear at the top of the current.

When wave signals are included in the calculations, the values of TKE, $\overline{p'w'}$, $\overline{\theta'w'}$, and σ_v are greater (more positive) than those obtained using only turbulence quantities. Our assumption that including wave perturbations in the second-order turbulence calculations leads to inflated statistics is confirmed for these quantities. This result suggests that closure schemes based on TKE may be inaccurate in the stable PBL if wave signals are not separated from the turbulence.

Because estimates of lateral plume dispersion, σ_v, can be falsely large if the wave signal $\tilde{v}$ is not removed, under-predictions of plume concentrations can occur. This can have serious consequences when estimating concentrations of hazardous materials in the air.

In Figs. 6 and 7, extreme values are seen at averaging times of about 10 min. Wave-like oscillations (not shown) with periods of about 10 min were seen in $(u - \bar{u})$ and $(w - \bar{w})$ between 0530 and 0600, and a disturbance with a period of about 10 min is seen in the wavelet analysis (Fig. 5) that was associated with the pressure jump. It is possible that the wave-like oscillations were due to a low-frequency wave produced by the pressure jump. Examining

Fig. 5 with high-resolution contours (not shown) shows wavelet energy at the 10-min scale about the time of the wave disturbance. We speculate that this wave-like disturbance, which was not filtered, appeared as turbulence in both methods of flux and variance calculations.

A correlation between σ_z and σ_w was observed in the lidar measurements, but this was expected. However, σ_z and $\tilde{w}$ showed little correlation. Also, fluctuations in the plume-centre height showed no correlation with $\tilde{w}$, and it is not known if a wave-turbulence interaction was operating. We know only that a wave and turbulence field were simultaneously present, though we cannot say that the fluctuations in the turbulence were directly related to the wave. There may have been other sources of turbulence fluctuations such as the 10-min wave-like disturbance. This suggests that in the often complex flows in the stable PBL, several mechanisms can contribute to the turbulence.

8 Conclusion

1. The methodology presented to decompose a signal q into its mean, turbulence, and wave components by using a band-pass filter to identify the wave component, $\tilde{q}$, is a practical method to analyse wave events that have non-constant amplitude and persist for only several cycles.
2. Comparison of the fluxes and variances calculated with and without the wave signal showed little differences when the averaging times were less than the wave period. Averaging times greater than the wave period showed wave-induced enhancements to second-order turbulence quantities.
3. Remotely-observed vertical dispersion of an elevated plume using a lidar showed σ_z and plume height were correlated with σ_w.
4. Observations in the stable PBL should identify and quantify wave-like disturbances.

Acknowledgements This research was supported by the U.S. Army Atmospheric Research Laboratory; the University of Connecticut, Storrs Agricultural Experiment Station; the New Mexico State University, Agriculture Experiments Station, and the NOAA Air Resources Laboratory, Atmospheric Turbulence and Diffusion Division. Additional thanks to Dr. Young Yee, U.S. Army Research Laboratory and Dr. Dragon Zajic, Arizona State University for providing the sodar and tethersonde data respectively.

References

De Baas AF, Driedonks GM (1985) Internal gravity waves in the stably stratified boundary layer. Boundary-Layer Meteorol 31:303–323

Einaudi F, Bedard AJ, Finnigan JJ (1989) A climatology of gravity waves and other coherent disturbances at the Boulder Atmospheric Observatory during March-April 1984. J Atmos Sci 46:303–329

Finnigan JJ (1988) Kinetic energy transfer between internal gravity waves and turbulence. J Atmos Sci 45:486–505

Finnigan J, Einaudi F (1993) Wave-turbulence dynamics in the stably stratified boundary layer. J Atmos Sci 50:1841–1864

Fritts DC, Nappo C, Riggin DM, Balsley BB, Eichinger WE, Newsom RK (2003) Analysis of ducted motions in the stable nocturnal boundary layer during CASES-99. J Atmos Sci 60:2450–2472

Hanna SR, Briggs GA, Hosker RP (1982) Handbook on Atmospheric Diffusion. DOE/TIC-11223 (DE82002045), Technical Information Center.U.S.Department of Energy. 102 pp

Hauf T, Finke U, Neisser J, Bull G, Stangenberg J.-G (1996) A ground-based network for atmospheric pressure fluctuations. J Atmos Ocean Technol 13:1001–1023

Hiscox AL, Miller DR, Nappo CJ, Ross J (2006a) Dispersion of fine spray from aerial applications in stable atmospheric conditions. Trans. Americ Soc Ag Bio Eng 49:1513–1520

Hiscox AL, Nappo CJ, Miller DR (2006b) On the use of lidar images of smoke plumes to measure dispersion parameters in the stable boundary layer. J Atmos Ocean Technol 23:1150–1154
Hussain AKFM, Reynolds WC (1972) The mechanics of an organized wave in a turbulent shear flow. J Fluid Mech 54:241–258
Koch SE, Golus RE (1988) A mesoscale gravity wave event observed during CCOPE. Part I: multiscale statistical analysis of wave characteristics. Mon Wea Rev 116:2527–2544
Lee X, Barr AG (1998) Climatology of gravity waves in a forest. Quart J Roy Meteorol Soc. 124:1403–1419
Nappo CJ (1991) Sporadic breakdowns of stability in the PBL over simple and complex terrain. Boundary-Layer Meteorol 54:69–87
Nappo CJ (2002) An Introduction to Atmospheric Gravity Waves. Academic Press, San Diego. 276 pp
Newsom R, Banta RM (2003) Shear-flow instability in the stable nocturnal boundary layer as observed by Doppler lidar during CASSES-99. J Atmos Sci 60:16–33
Rao KS, Nappo CJ (1998) Turbulence and dispersion in the stable atmospheric boundary Layer. In:Singh MP, Raman S (eds) Dynamics of atmospheric flows: atmospheric transport and diffusion processes Computational Mechanics Publications, Southampton, pp.39–91
Rees JM, Denholm-Price JCW, King JC, Anderson PS (2000) A clomatological study of internal gravity waves in the atmospheric boundary layer overlying the Brunt ice shelf, Antarctica. J Atmos Sci 57:511–526
Steeneveld GJ, Holtslag AAM, Nappo CJ, van de Wiel BJH, Mahrt L (2008) Exploring the possible role of small scale terrain drag on stable boundary layers over land. J Appl Meteorol Clim. doi:10.1175/2008JAMC1816.1
Sun J, Lenschow DH, Burns SP et al (2002) Intermittent turbulence associated with a density current passage in the stable boundary layer. Boundary-Layer Meteorol 105:199–219
Sun J, Lenschow DH, Burns SP et al (2004) Atmospheric disturbances that generate intermittent turbulence in nocturnal boundary layers. Boundary-Layer Meteorol 110:255–279
Torrence CT, Compo GP (1998) A practical guide to wavelet analysis. Bull Am Meteol Soc 79:61–78
Zilitinkevich SS (2002) Third-order transport due to internal waves and non-local turbulence in the stably stratified surface layer. Quart J Roy Meterol Soc 128:913–925